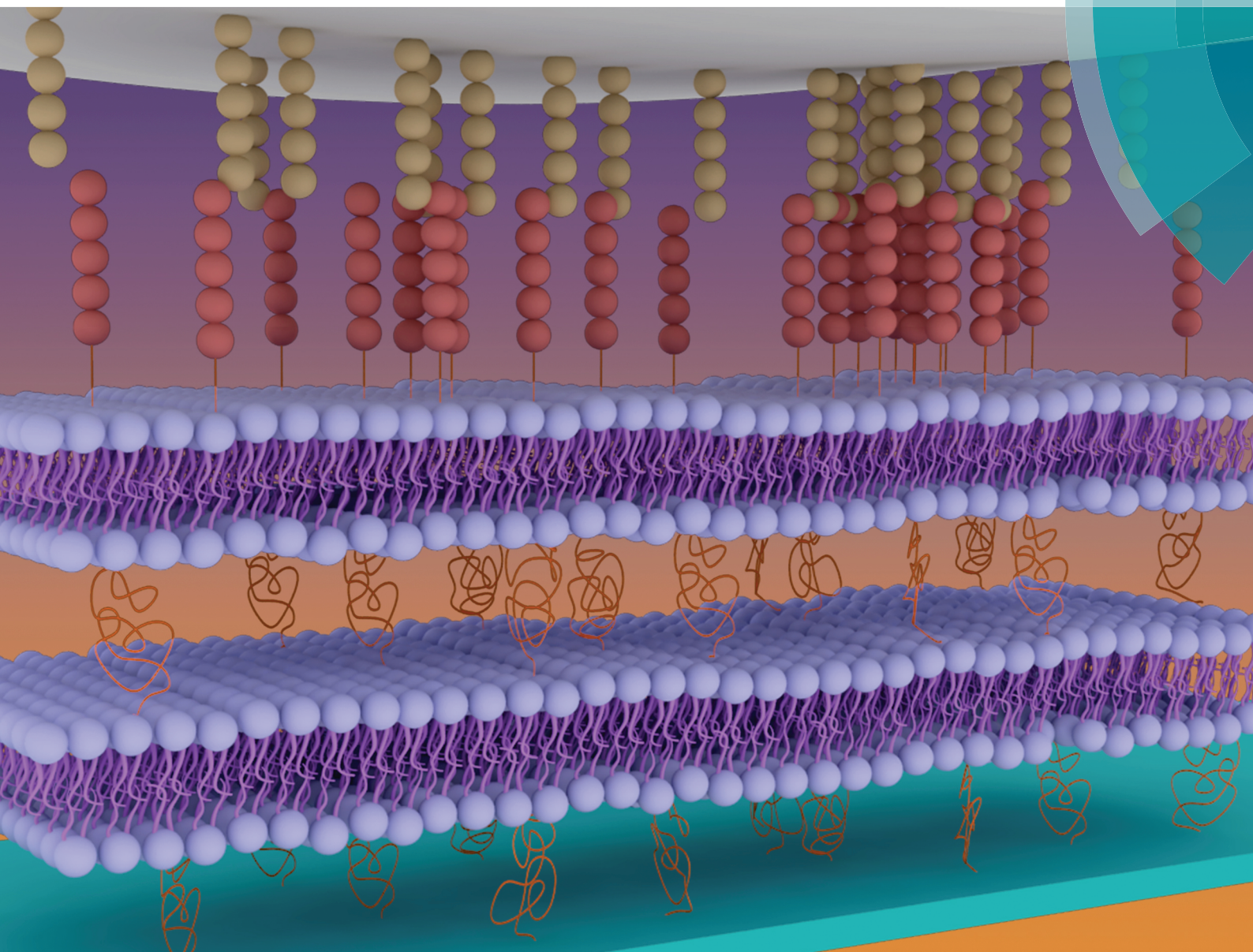


# Soft Matter

www.softmatter.org



ISSN 1744-683X



ROYAL SOCIETY  
OF CHEMISTRY

PAPER

C. A. Naumann *et al.*

N-cadherin-functionalized polymer-tethered multi-bilayer: a cell surface-mimicking substrate to probe cellular mechanosensitivity

**175**  
YEARS



Cite this: *Soft Matter*, 2016,  
12, 8274

## N-cadherin-functionalized polymer-tethered multi-bilayer: a cell surface-mimicking substrate to probe cellular mechanosensitivity

Y. Ge,<sup>a</sup> Y. H. Lin,<sup>a</sup> L. A. Lautscham,<sup>b</sup> W. H. Goldmann,<sup>b</sup> B. Fabry<sup>b</sup> and C. A. Naumann<sup>\*a</sup>

Fate and function of anchorage-dependent cells depend on a variety of environmental cues, including those of mechanical nature. Previous progress in the understanding of cellular mechanosensitivity has been closely linked to the availability of artificial cell substrates of adjustable viscoelasticity, allowing for a direct correlation between substrate stiffness and cell response. Exemplary, polymeric gel substrates with polymer-conjugated cell-substrate linkers provided valuable insight into the role of mechanical signals during cell migration in an extracellular matrix environment. In contrast, less is known about the role of external mechanical signals across cell–cell interfaces, in part, due to the limitations of traditional polymeric substrates to mimic the remarkable dynamics of cell–cell linkages. To overcome this shortcoming, we introduce a cell surface-mimicking cell substrate of adjustable stiffness, which is comprised of a polymer-tethered lipid multi-bilayer stack with N-cadherin linkers. Unlike traditional polymeric cell substrates with polymer-conjugated linkers, this novel artificial cell substrate is able to replicate the dynamic assembly/disassembly of cadherin linkers into linker clusters and the long-range movements of cadherin-based cell-substrate linkages observed at cell–cell interfaces. Moreover, substrate stiffness can be changed by adjusting the number of bilayers in the multi-bilayer stack, thus enabling the analysis of cellular mechanosensitivity in the presence of artificial cell–cell linkages. The presented biomembrane-mimicking cell substrate provides a valuable tool to explore the functional role of mechanical cues from neighboring cells.

Received 21st July 2016,  
Accepted 19th August 2016

DOI: 10.1039/c6sm01673a

[www.rsc.org/softmatter](http://www.rsc.org/softmatter)

### Introduction

Cell migration is important for a wide range of cellular processes, such as embryonic development, immune response, wound healing, and metastasis of cancer cells. During cell migration, actomyosin-induced contractile forces are transduced to the cell substrate/surrounding matrix at cellular adhesions, such as integrin-based focal adhesions (FAs) and cadherin-based adherens junctions (AJs).<sup>1–4</sup> Cells migrating in an extracellular matrix (ECM) environment such as collagen substrates typically show stationary FAs, although inward-sliding FAs may occur at the cell's tail.<sup>5,6</sup> In contrast, AJs of migrating cells may display a remarkable long-range dynamics, which includes basal-to-apical flow and tread-milling movements of AJs between polarized cells.<sup>7,8</sup> Importantly, both types of cellular adhesions act as mechanical sensors, which adapt their size and shape to

external mechanical cues by assembly/disassembly of adhesion proteins.<sup>4,9,10</sup> This assembly/disassembly process is mediated by a large number of associated proteins, such as FAs-associated proteins talin, vinculin, FAK, zyxin, and paxilin and AJs-associated proteins  $\alpha$ -catenin,  $\beta$ -catenin, and vinculin, which dynamically regulate the linkage between adhesion receptors and cytoskeleton.<sup>11–14</sup> Migrating cells are not only able to detect mechanical signals from their surrounding,<sup>15</sup> but also transduce these signals into biochemical responses through a process known as cellular mechanotransduction.<sup>16</sup> There is a relationship between modifications of cellular mechanotransduction and disease.<sup>17,18</sup> Another example for the importance of cellular mechanosensitivity is stem cell differentiation, which depends on substrate stiffness.<sup>19</sup> However, while processes of cellular mechanosensitivity during cell migration in an ECM environment are now well characterized, less is known about the mechanisms and significance of such processes across cell–cell interfaces.<sup>20</sup>

Recent advances in understanding the mechanosensitivity of migrating cells have been closely linked to the development of artificial cell substrates of adjustable viscoelasticity, allowing for direct correlation between substrate stiffness and cell response.

<sup>a</sup> Department of Chemistry and Chemical Biology, Indiana University-Purdue University, Indianapolis, 46202 USA. E-mail: [canauman@iupui.edu](mailto:canauman@iupui.edu)

<sup>b</sup> Department of Biophysics, University of Erlangen-Nuremberg, Erlangen, 91052, Germany

In particular, this concept has been successfully applied using ECM mimetics comprised of artificial polymeric gels of adjustable crosslinking density carrying ECM protein or ECM protein-mimicking peptide linkers.<sup>21</sup> To create a cell surface-like environment, polymeric gel substrates with cadherin linkers have been developed.<sup>22,23</sup> However, such a cell surface mimetic cannot replicate the linkage mobility found at cellular adhesions. Planar membrane systems, such as patterned or unpatterned solid-supported single lipid bilayers or single bilayers of diblock copolymers with mobile linkers, have been introduced.<sup>24–27</sup> However, the inability to adjust substrate stiffness makes these biomembrane-mimicking substrates less suitable for the analysis of cellular mechanosensitivity.

Here we introduce a polymer-tethered lipid multi-bilayer with N-cadherin linkers to overcome the limitations of existing cell surface-mimicking cell substrates for the analysis of cell migration and cellular mechanosensitivity. Our experiments demonstrate that, unlike traditional polymeric gel substrates, polymer-tethered lipid multi-bilayers enable the dynamic assembly of linkers into linker clusters at cellular adhesions without impairing cell spreading and migration. Furthermore, we confirm earlier experiments on laminin-coated polymer-tethered lipid multi-bilayers<sup>28,29</sup> and show that this bio-inspired membrane architecture allows for the adjustment of substrate viscoelasticity by altering the number of stacked bilayers, providing a key tool for the analysis of cellular mechanosensitivity. Specifically, we demonstrate that changes in bilayer stacking lead to significant changes in cytoskeletal organization, AJ formation, motility, and cellular traction forces of C2C12 myoblasts, illustrating that AJ-like N-cadherin junctions between cells and substrate are highly mechanosensitive. Our experiments establish that N-cadherin-functionalized polymer-tethered lipid multi-bilayers provide valuable insight into the spatio-temporal development of cell–cell linkages between migrating cells in response to external mechanical stimuli.

## Materials and methods

### Multi-bilayer fabrication

Stacks of multiple polymer-tethered lipid bilayers were fabricated as described previously.<sup>30</sup> In short, the layer-by-layer assembly of the polymer-tethered multi-bilayer stack was accomplished through subsequent addition of giant unilamellar vesicles (GUVs) consisting of either 1-palmitoyl-2-oleoyl-*sn*-glycero-3-phosphocholine (POPC) and 5 mol% 1,2-dipalmitoyl-*sn*-glycero-3-phosphothioethanol (DPTE) or POPC and 5 mol% 1,2-distearoyl-*sn*-glycero-3-phosphoethanolamine-*N*-[maleimide(polyethylene glycol)2000] (ammonium salt) (PEG2000-maleimide). All lipids and lipopolymers were purchased from Avanti Polar Lipids (Alabaster, AL). Maleimide–thiol coupling between DPTE and PEG200-maleimide lead to stable linkages between adjacent lipid bilayers. To assist this process, GUVs contained 0.1 mM sucrose/1 mM CaCl<sub>2</sub>, thus promoting their transport to the substrate *via* gravitation. For each planar bilayer addition, GUVs were allowed to bind and unfold for 2–4 h followed by rinsing with Milli-Q to remove

excess GUVs. To facilitate formation of cadherin–cadherin linkages between multi-bilayer substrate and plated cells, GUVs forming the top bilayer also contained 0.5 mol% of the Ni-chelator lipid 1,2-dioleoyl-*sn*-glycero-3-[[*N*-(5-amino-1-carboxypentyl)iminodiacetic acid)succinyl] (nickel salt) (DGS-NTA Ni) (Avanti Polar Lipids, Alabaster, AL); GUV addition was conducted in calcium ion-free buffer. In a subsequent step, an equimolar ratio (relative to DGS-NTA Ni) of His-tagged N-cadherin chimeras (R&D Systems, Minneapolis, MN) was added and allowed to bind to DGS-NTA Ni in the top bilayer of the multi-bilayer system (incubation time: 30 min). Next, the bilayer sample was rinsed with PBS to remove unbound N-cadherin chimera. To confirm the distribution and lateral mobility of bilayer-bound N-cadherin chimera in the absence of plated cells, Alexa 555-labeled anti-N-cadherin antibodies (Thermo Fisher Sci. Waltham, MA) were added in excess (antibody-to-chimera ratio: 1.5 : 1) and allowed to bind to the functionalized polymer-tethered lipid bilayer sample using an incubation time of 1.5 h followed by rinsing off excess (unbound) antibodies with PBS. Dye-labeling of antibodies using an Alexa 555 antibody labeling kit (Life Technologies/Invitrogen, Carlsbad, CA) followed standard procedures. Alternative, N-cadherin chimera were fluorescently labeled using a commercial Alexa Fluor-555 protein labeling kit (Invitrogen, Carlsbad, CA) to visualize their distribution underneath plated cells. Laminin linkers were formed by linking mouse laminin (Invitrogen, Carlsbad, CA) to DPTE in the top bilayer *via* the heterobifunctional maleimide–NHS ester crosslinker *N*-gamma-maleimidobutryloxysulfosuccinimide (Sulfo-GMBS) (Thermo Scientific, Rockford, IL), as described previously.<sup>29</sup> To confirm the presence and integrity of the bilayer using fluorescence microscopy, the top bilayer of the multi-bilayer stack typically also contained 0.5 mol% of the fluorescently labeled lipid Texas Red-1,2-dihexadecanoyl-*sn*-glycero-3-phosphoethanolamine (TR-DHPE) (Invitrogen, Carlsbad, CA). In the absence of plated cells, some fluorescence analysis experiments were also conducted using the dye-labeled lipid *N*-(7-nitrobenz-2-oxa-1,3-diazol-4-yl)-1,2-dihexadecanoyl-*sn*-glycero-3-phosphoethanolamine, triethylammonium salt (NBD-DHPE) (Invitrogen, Carlsbad, CA).

### Cell culture

C2C12 myoblasts (ATCC, Manassas, VA) were cultured in Dulbecco's Modified Eagle Medium (DMEM) (Invitrogen Life Science, Carlsbad, CA) with 10% fetal bovine serum (Thermo Fisher Sci., MA) and 100 U mL<sup>-1</sup> penicillin/streptomycin (Thermo Fisher Sci., MA). Cells were incubated at 37 °C in a humidified 5% CO<sub>2</sub> atmosphere and passaged every two days. Prior to plating, cells were passaged at least twice and not more than 12 times. For cell passaging, 2.5% trypsin (Thermo Fisher Sci., Rockford, IL) was employed to detach C2C12 myoblasts from the surface of 75 μL or 25 μL culture flask (BD BioScience, CA). Prior to plating, cells were rinsed with PBS and trypsinized using 0.25% trypsin/EDTA. In typical experiments, cells were plated at a density of 80 mm<sup>-2</sup>. The viability of plated cells (incubation at 37 °C and 5% CO<sub>2</sub> for 20 and 40 h) was tested using an Invitrogen LIVE/CELL assay. Here 200 μL of LIVE/DEAD viability stock solution (Invitrogen Life Science, Carlsbad, CA) was added to the sample

to cover all cells and following an incubation time of 40 min, the samples were rinsed with PBS buffer and observed through the FITC (live cell detection) and Alexa 555 channels (dead cell detection) of a confocal microscope (FV 1000, Olympus USA, Center Valley PA).

### Polyacrylamide gels

Polyacrylamide (PAA) gels were cast on pretreated glass slides. Pretreatment of glass slides included subsequent incubation in aqueous solutions (0.1 M NaOH, 2.0% 3-aminopropyltrimethoxysilane, and 2.5% glutaraldehyde) and rinsing with Milli-Q water after each incubation step. Formation of the PAA gel followed established procedures.<sup>31,32</sup> In short, aqueous solutions with 40% acrylamide/bisacrylamide with embedded 500 nm green fluorescent beads (505/515) (Invitrogen/Life Science, Carlsbad, CA) were used to achieve final concentrations of 4.1% or 6.1% acrylamide. The solution was centrifuged at 1500 rpm for 30 min at 4 °C, and 0.2% *N,N,N',N'*-tetramethylethylenediamine (TEMED) was added as a cross-linker and mixed with the initiator (0.5% ammonium persulfate, APS) to start the polymerization and crosslinking reactions at room temperature for 1 h. For activation of the gel surface, 150  $\mu$ L of the photo crosslinker Sulfo-SANPHA (Thermo Fisher Sci. Rockford, IL) was added and allowed to bind to the gel using UV light irradiation for 5 min. After extensive rinsing with PBS to remove unbound Sulfo-SANPHA, 120  $\mu$ L of 1.5% fibronectin solution (Thermo Fisher Sci. Rockford, IL) was added and incubated overnight to allow fibronectin binding to the gel *via* Sulfo-SANPHA linkers. Prior to usage, the gel was stored in PBS buffer at 4 °C for up to 4 days.

### Microscopy techniques (bilayer characterization without plated cells)

A Confocor 2 microscopy system (Carl Zeiss, Jena, Germany) equipped with an Axiovert 200M (Carl Zeiss, Oberkochen, Germany), a Zeiss C-Apochromat objective (water immersion, 40 $\times$  NA = 1.2), and a Zeiss AxioCam MRm monochrome digital camera was utilized to analyze the distribution, aggregation state, and lateral mobility of Alexa 555-antibody-labeled cadherin linkers in the various multi-bilayer systems. In addition to epifluorescence (EPI), the microscopy system was also equipped with confocal fluorescence correlation spectroscopy (FCS) and photon counting histogram analysis (PCH).<sup>33</sup> EPI was employed to characterize the distribution of dye-antibody-labeled N-cadherin chimera in the bilayer. FCS autocorrelation analysis was utilized to determine the average brightness and lateral mobility of Alexa 555-labeled MAbs in solution and bound to bilayer-reconstituted N-cadherin linkers. For FCS studies on planar bilayer systems, the confocal spot was kept at a fixed bilayer position, and the photon counts through the Alexa 555 channel were collected over 50 s. The correct confocal position was obtained by maximizing the photon-count rate of the probe molecule of interest. As reported before, diffusion coefficients of bilayer-incorporated probe molecules were determined using a TRITC-DHPE standard, for which the FCS diffusion time could be compared to a diffusion coefficient determined using wide-field single molecule fluorescence microscopy.<sup>34</sup> This approach was chosen because

uncertainties about the exact geometry of the confocal spot limit the accuracy of lateral diffusion coefficients of probe molecules directly obtained from FCS autocorrelation analysis. Raw data of photon counts at a fixed bilayer position were also analyzed using the PCH method. This method was used to determine the average brightness and number of Alexa 555 antibody-tagged N-cadherin monomers ( $\epsilon$ ,  $N_{\text{avg}}$ ) and dimers ( $\epsilon_{\text{dimer}} (= 2\epsilon)$ ,  $N_{\text{avg,dimer}}$ ) in the bilayer system by adapting methods reported previously.<sup>33</sup> The dimerization level can be quantified in terms of the mole fraction of dimers,  $x_{\text{dimer}}$ . The accuracy of the PCH method was previously tested using fluorescent dyes and CdSe/ZnS quantum dots in solution and bound to lipids in a planar lipid bilayer.<sup>33</sup>

### Live cell imaging

Live cell imaging experiments on C2C12 myoblasts were conducted 20 h after plating using a FV1000 confocal microscopy system (Olympus USA, Center Valley, PA) equipped with an active z-axial drift correction system (ZDC, Olympus USA, Center Valley, PA) to enable long-term studies and a stage cell incubator (Takashi Thermo, Japan) for live cell studies operated at 37 °C and 5% CO<sub>2</sub>. Confocal micrographs of plated cells were acquired through a 20 $\times$  objective (Olympus USA, UPlanSAPO 20 $\times$ /0.75), using Olympus FV10-ASW imaging software (Olympus USA, Center Valley, PA). Micrographs were analyzed in terms of cell spreading area and extent of stress fiber formation using FV10-ASW viewer software (Olympus USA, Center Valley, PA). To determine cell migration speed, confocal micrographs of plated cells were acquired every 5 min over a time period of 2 h. Cell motility data were obtained by tracking the nucleus of migrating cells over time using ImageJ and the plugin "object tracker and manual tracking".

Fluorescent recovery after photo-bleaching (FRAP) assays were applied to determine the diffusion coefficient,  $D$ , and immobile fraction,  $IF$ , of fluorescently-labeled N-cadherin chimera and TR-DHPE in the polymer-tethered multi-bilayer. Specifically, FRAP assays were performed with a FV1000 confocal microscopy system (Olympus USA, Center Valley, PA), equipped with 60 $\times$  UPlanSAPO water-immersion objective (NA: 1.15) and INU-ZILCS-F1 stage incubator (Tokai Hit, Shizuoka-ken, Japan). Data were acquired using the diffusion analysis package of the Olympus FV10-ASW imaging software (Olympus USA, Center Valley, PA). Dye-labeled N-cadherin and TR-DHPE in the bilayer were bleached with maximum laser power using the tornado scanning mode of the confocal system, resulting in a well-defined bleaching spot of 1  $\mu$ m diameter. Image acquisition started 2 min before bleaching and continued for up to 6 min at a rate of one image every 20 seconds. Acquired FRAP data were background-corrected and fitted using a single exponential model.<sup>35</sup>

### Immunofluorescence

Immunofluorescence experiments were conducted to characterize actin network organization and AJs by adapting procedures described before.<sup>28</sup> Typically, about 8.5 cells per mm<sup>2</sup> were cultured for 20 h at 37 °C and 5% CO<sub>2</sub> on laminin-coated glass or multi-bilayer substrates with laminin or N-cadherin linkers inside of a 35 mm petri dish with a 15 mm diameter glass bottom.

Cells were fixed in 4% formaldehyde and treated with 0.5% Triton X-100 (incubation time for each step: 10 min) followed by rinsing with PBS and 1 h incubation in PBS with 1% BSA. The AJs marker  $\beta$ -catenin was fluorescently labeled using an Alexa 488-labeled anti- $\beta$ -catenin antibody (eBioscience, San Diego, CA). Actin was labeled by sequential addition of primary anti-paxillin antibody (BD Bioscience, San Jose, CA) and secondary IgG1 antibody (BD Bioscience, San Jose, CA) labeled with phalloidin-TRITC (Sigma Aldrich, St. Louis, MO). Samples were washed with PBS and 3% BSA in PBS and stored at 4 °C until used. Fluorescently labeled cells were imaged using confocal microscopy (FV1000, Olympus USA, Center Valley, PA) and analyzed using Olympus FV10-ASW imaging software and Image J.

### Traction force microscopy

A modified traction force microscopy assay was employed to probe cellular traction forces in a PAA gel underneath biomembrane-mimicking cell substrates using procedures described previously.<sup>28</sup> In short, after preparation of the PAA gel with a Young's modulus of 11.3 kPa that contains embedded fluorescent particles and a fibronectin surface coating (described in Section 2.3), linkage between lipid bilayer and fibronectin layer was accomplished by subsequently adding hetero-bifunctional NHS-maleimide crosslinker Sulfo-GMBS (Thermo Fisher Sci. Rockford, IL) (concentration: 10 mg mL<sup>-1</sup> in DMSO; incubation time: 30 min) and lipid bilayer containing POPC and 5 mol% DPTE. Formation of multi-bilayers and design of bilayer-cell linkers followed procedures described earlier. C2C12 myoblasts were placed on the bilayer-functionalized gels at a density of 80 cells per mm<sup>2</sup> and incubated at 37 °C and 5% CO<sub>2</sub>. Bright-field images of plated cells were acquired together with fluorescent micrographs (through FITC channel) of bead positions 20 hours after plating using an inverted optical microscope (Axiovert 200M, Carl Zeiss, Oberkochen, Germany) with EC Plan-NEOFLUAR objective (20 $\times$ , NA = 0.5) (Carl Zeiss, Jena, Germany). Following the treatment of cells with a 100  $\mu$ L cocktail of 80  $\mu$ M cytochalasin D (BD BioScience, CA) in 0.25% trypsin solution to relax cell forces, fluorescent micrographs of the bead positions were taken again. The displacement of beads after force relaxations was analyzed with a particle tracking algorithm described by Raupach *et al.*<sup>36</sup> Traction forces were calculated using the Fourier transform traction cytometry method.<sup>37</sup> Furthermore, the strain energy of cells was estimated using a methodology previously described in Koch *et al.*<sup>32</sup>

## Results and discussion

### Laterally mobile N-cadherin chimera become immobilized upon induced clustering in polymer-tethered lipid bilayer

Upon fabrication of the linker-functionalized polymer-tethered lipid multi-bilayer substrate described in the Materials and methods section, the homogeneity of the bilayer system and the distribution of bilayer-bound N-cadherin chimera, which consists of the ectodomain of N-cadherin with a His-tag enabling binding to DGS-NTA Ni lipids in the bilayer, were first

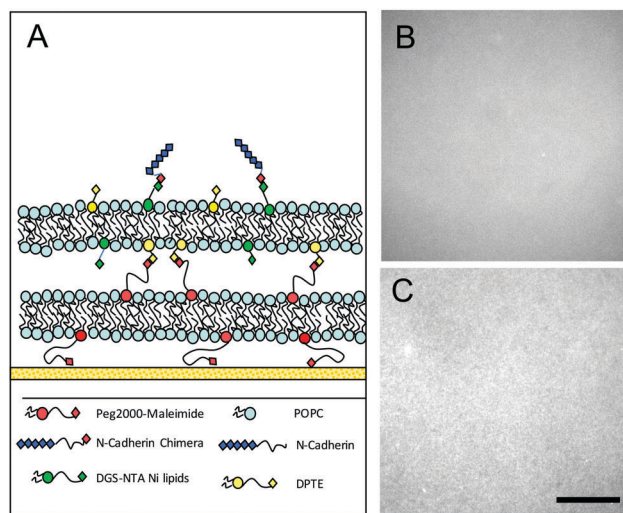


Fig. 1 Design of polymer-tethered double bilayer with N-cadherin chimera (A) and EPI micrographs of TRITC-DHPE (B) and fluorescently tagged N-cadherin chimera (C) in such a membrane system prior to cell plating. Scale bar: 50  $\mu$ m.

examined in the absence of plated cells using fluorescence microscopy (Fig. 1A). Here, EPI fluorescence analysis of TRITC-DHPE distribution in the top bilayer of a double bilayer system confirmed the formation of a homogeneous second (top) bilayer in the double bilayer system (Fig. 1B), which is in good agreement with earlier findings on comparable bilayer systems.<sup>29,30</sup> Furthermore, the featureless EPI micrograph of bilayer-bound N-cadherin chimera (labeled with Alexa 555-anti-N-cadherin antibody) illustrates their homogeneous distribution in the bilayer prior to cell plating (Fig. 1C).

Next, we acquired time scans of confocal fluorescence count rates of N-cadherin chimera (labeled using Alexa 555 anti-N-cadherin antibody) at fixed positions on a polymer-tethered lipid bilayer in Ca<sup>2+</sup>-free PBS (Fig. 2A). The peaks in Fig. 2A demonstrate the lateral mobility of dye-labeled N-cadherin chimera in the bilayer, as they reflect the passage of these probe molecules through the confocal volume. Analysis of the time evolution of the fluorescence count rate using FCS auto-correlation analysis provided a lateral diffusion coefficient of  $D(\text{N-cadherin chimera}) = 0.34 \pm 0.05 \mu\text{m}^2 \text{s}^{-1}$  (Fig. 2B), which is in good agreement with previously reported diffusion results of cadherin-chimera in a supported lipid bilayer.<sup>38</sup> Complementary analysis of the time scans of confocal fluorescence intensity using the PCH method shows that  $x_{\text{dimer}}(\text{N-cadherin chimera}) = 0.16 \pm 0.01$  (Fig. 2C), demonstrating the predominantly monomeric nature of N-cadherin chimera in the bilayer. Together, the data in Fig. 2B and C indicate the largely viscous behavior of the polymer-tethered multi-bilayer system with respect to individual lipid-bound linkers, such as N-cadherin chimera.

To examine the lateral mobility of N-cadherin chimera clusters in the polymer-tethered lipid bilayer system, N-cadherin chimera-functionalized fluorescent beads (size: 500 nm) were allowed to bind to polymer-tethered lipid bilayers containing 0.1 mol% N-cadherin chimera (Fig. 3A) by adapting procedures reported

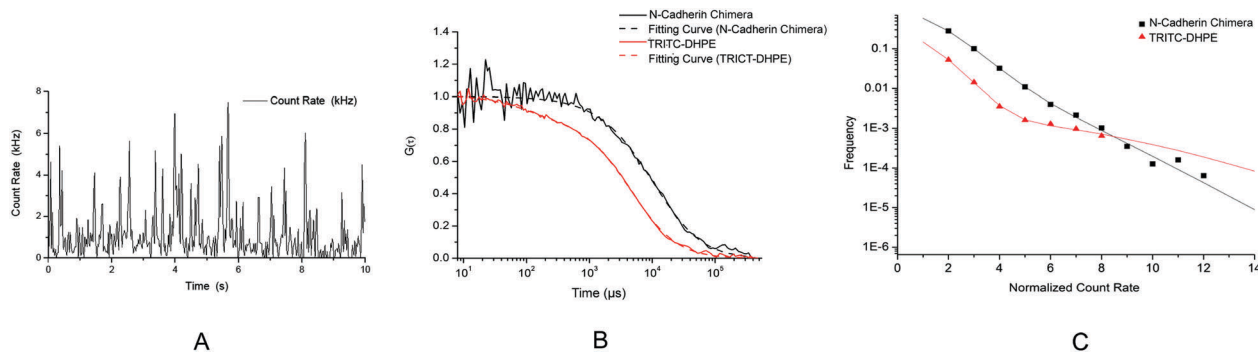


Fig. 2 Confocal count rate of fluorescently tagged N-cadherin chimera in a polymer-tethered bilayer system in PBS (without  $\text{Ca}^{2+}$ ) over time (A). FCS autocorrelation (B) and PCH analyses (C) of confocal count rate provided  $D(\text{N-cadherin chimera}) = 0.34 \pm 0.05 \mu\text{m}^2 \text{s}^{-1}$  and  $x_{\text{dimer}}(\text{N-cadherin chimera}) = 0.16 \pm 0.01$ , respectively. Corresponding FCS and PCH analyses of TRITC-DHPE (used as reference) in a comparable membrane environment resulted in  $D(\text{TRITC-DHPE}) = 1.66 \pm 0.39 \mu\text{m}^2 \text{s}^{-1}$  and  $x_{\text{dimer}}(\text{TRITC-DHPE}) = 0.018 \pm 0.012$ , respectively.

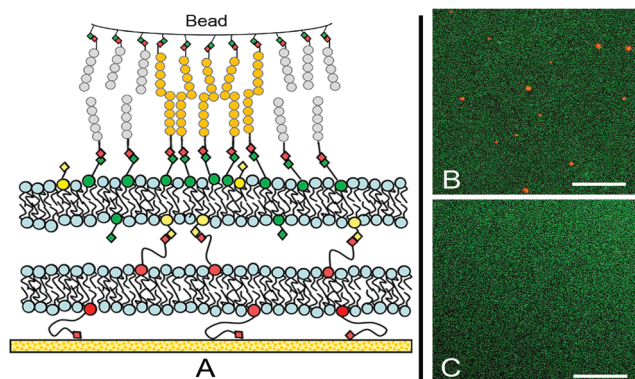


Fig. 3 Schematic of N-cadherin chimera-functionalized fluorescent bead in the presence of a polymer-tethered multi-bilayer with bilayer-bound N-cadherin chimera (A). Representative dual-color fluorescent micrograph showing binding of N-cadherin-functionalized fluorescent (red) beads on a such a membrane system in the presence of  $\text{PBS}-\text{CaCl}_2$  (1 mM) [top bilayer labeled with 0.6 mol% NBD-DHPE (Invitrogen)]; image taken following an incubation time of 2 h and extensive rinsing with  $\text{PBS}-\text{CaCl}_2$  (1 mM) solution] (B). In contrast, N-cadherin chimera-functionalized fluorescent beads do not bind to the same type of functionalized bilayer in  $\text{Ca}^{2+}$ -free solution (C). Scale bar: 5  $\mu\text{m}$ .

before.<sup>39</sup> As the fluorescence micrograph in Fig. 3B illustrates, N-cadherin chimera-functionalized beads were able to bind on N-cadherin chimera-functionalized bilayer substrates in the presence of  $\text{Ca}^{2+}$ . In contrast, comparable beads neither did bind to the same type of functionalized bilayer in the absence of  $\text{Ca}^{2+}$  (Fig. 3C) nor did they bind to the linker-free bilayer (data not shown), demonstrating a high specificity of this binding process. Unlike individual, laterally mobile N-cadherin-chimera described in Fig. 2, N-cadherin chimera-functionalized fluorescent beads are completely immobilized upon binding to the N-cadherin chimera-functionalized polymer-tethered multi-bilayer, suggesting an elastic materials response of the polymer-tethered membrane with respect to N-cadherin chimera clusters. The observed immobilization of N-cadherin chimera clusters in the polymer-tethered membrane environment highlights the important role of lipopolymers in the regulation of probe diffusivity in the polymer-tethered lipid bilayer.<sup>40,41</sup> For example, comparable

changes in probe size, due to clustering, have a notably weaker effect on probe diffusivity in a viscous supported fluid lipid bilayer without polymer-tethered lipids.<sup>42</sup>

### C2C12 myoblasts are able to adhere and spread on N-cadherin chimera-functionalized polymer-tethered lipid bilayer

Next, myoblast adhesion and spreading on a polymer-tethered double bilayer system was investigated in the absence (Fig. 4A) and presence (Fig. 4B and C) of N-cadherin chimera using DIC microscopy to confirm the functionality as a cell substrate. On the N-cadherin chimera-free cell substrate, myoblasts maintain a spherical shape (20 h after plating), indicating their inability to adhere (Fig. 4A). In contrast, C2C12 myoblasts spread well on corresponding double bilayer substrates containing N-cadherin chimera concentrations of 0.1 mol% (Fig. 4B) and 0.04 mol% (Fig. 4C), which correspond to average N-cadherin chimera distances of 48 and 68 nm, respectively. Analysis of about 60 cells for each N-cadherin chimera density provides almost identical projected cell areas of  $104 \pm 35 \mu\text{m}^2$  (0.1 mol%) and  $108 \pm 41 \mu\text{m}^2$  (0.04 mol%). This finding is remarkable in comparison to previous cell spreading results obtained on polymeric substrates with

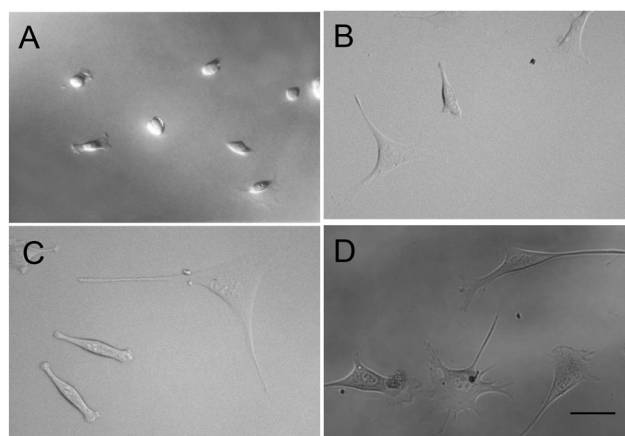


Fig. 4 C2C12 myoblasts on a polymer-tethered bilayer system with different linkers. (A) No linker; (B) 0.1 mol% N-cadherin chimera; (C) 0.04 mol% N-cadherin chimera; (D) 0.1 mol% laminin. Scale bar: 20  $\mu\text{m}$ .

immobilized linkers, which exhibit enhanced projected cell areas with increasing linker density below a critical linker distance of  $\sim 70$  nm.<sup>43</sup> As Fig. 4D illustrates, C2C12 myoblasts also display good spreading behavior on a polymer-tethered lipid multi-bilayer, in which N-cadherin chimera are replaced by laminin (laminin molar concentration relative to lipids: 0.1 mol%). Here, systematic analysis of the cell spreading area of at least 80 cells reveals that plated C2C12 cells exhibit a  $33 \pm 3\%$  higher spreading area on polymer-tethered multi-bilayers with laminin linkers *versus* N-cadherin chimera linkers. Differences in cell spreading on polymer-tethered multi-bilayers with laminin *versus* N-cadherin chimera linkers can be attributed to the different material properties of both linker coatings. While laminin linkers are able to form an elastic laminin network on top of the polymer-tethered lipid multi-bilayer system,<sup>44</sup> the FCS data in Fig. 2B suggest that a comparable elastic network formation of N-cadherin chimera linkers on such a multi-bilayer substrate can be excluded.

C2C12 myoblasts in a  $\text{Ca}^{2+}$ -containing medium readily spread and migrate on a polymer-tethered lipid bilayer substrate with N-cadherin chimera linkers, whereas C2C12 myoblast spreading is suppressed on comparable substrates in a  $\text{Ca}^{2+}$ -free medium or on corresponding linker-free substrates. These findings indicate the formation of N-cadherin linkages between adherent cells and substrate. To form such linkages in the polymer-tethered multi-bilayer system, individual N-cadherin chimera linkers should be able to assemble into linker clusters at cell-substrate linkage sites.<sup>4</sup> Notably, similar assembly processes have been considered to explain the remarkable dynamics and plasticity of AJs during cellular mechanosensing. For example, it is known that AJ formation requires the lateral mobility of individual cadherins in the plasma membrane.<sup>45,46</sup> Previous FRAP experiments also revealed the slow turnover of cadherin receptors at cell-bead contacts.<sup>13</sup> Another study reported that cadherins leave cell-cell junctions by switching their adhesive bond.<sup>47</sup> Traditional linker-functionalized polymeric cell substrates are limited in their ability to mimic the dynamic assembly/disassembly of linkers during maturation of cellular adhesion sites.

#### N-cadherin chimera accumulate and assemble into clusters underneath adhered C2C12 myoblasts

We next explored the distribution and lateral mobility of fluorescently labeled N-cadherin chimera and lipids (TR-DHPE) in a polymer-tethered lipid bilayer in the presence of plated C2C12 myoblasts. As illustrated in Fig. 5A, the presence of adherent cells does not alter the homogeneous distribution of TR-DHPE in the bilayer. This finding illustrates the integrity of the polymer-tethered lipid multi-bilayer in the presence of plated cells, which is in excellent agreement with earlier results on comparable membrane systems with laminin linkers.<sup>29</sup> Corresponding FRAP analysis of TR-DHPE mobility underneath spreading cells provides a diffusion coefficient of  $D = 1.67 \pm 0.05 \mu\text{m}^2 \text{s}^{-1}$  and almost complete fluorescence recovery (IF = 9%), indicating the lateral mobility of individual lipids in such a membrane environment (Fig. 5B). These FRAP results are consistent with previously reported lipid diffusion data determined in comparable membrane architectures.<sup>41</sup> Remarkably, in contrast

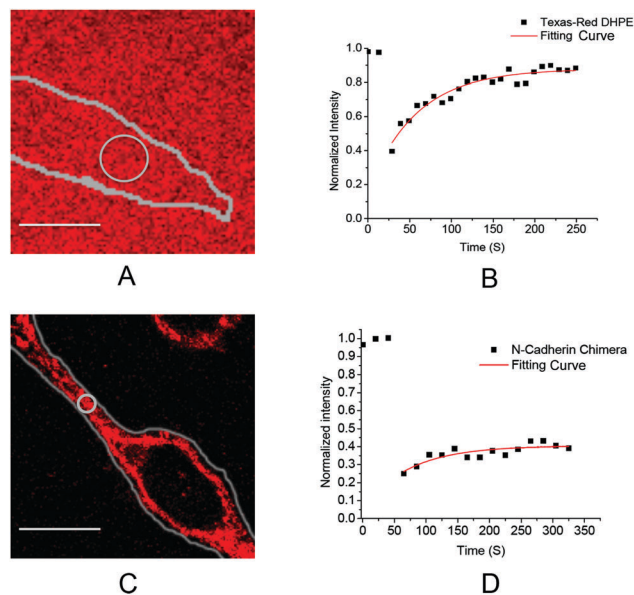


Fig. 5 Plated cells do not alter the distribution of TR-DHPE in a N-cadherin chimera-functionalized polymer-tethered bilayer substrate (A). FRAP analysis of TR-DHPE reveals nearly full fluorescence recovery underneath plated cells (B). In contrast, Alexa-555 labeled N-cadherin chimera on comparable substrates accumulate underneath plated cells (C). FRAP analysis of N-cadherin chimera shows only partial recovery (D). FRAP data were fitted using a single exponential model. Contour of plated cells is indicated by a line; location of bleached area is shown as a circle. Scale bar:  $5 \mu\text{m}$ .

to TR-DHPE, N-cadherin chimera accumulate in the bilayer region occupied by adherent cells (Fig. 5C). Fig. 5C also shows that N-cadherin chimera underneath plated cells are heterogeneously distributed, thereby exhibiting enrichment at the periphery and extensions of the migrating cell. This heterogeneous N-cadherin chimera distribution reflects the actual adhesion regions between cell and substrate, as illustrated by comparable ring-like enrichments of linkages between linker-functionalized supported fluid lipid bilayers and adsorbed vesicles.<sup>48</sup> Accompanying FRAP analysis of dye-labeled N-cadherin chimera in bilayer regions occupied by plated cells confirms a partial fluorescence recovery with a substantial immobile fraction of IF = 59.5% and a diffusion coefficient of the mobile fraction of  $D = 0.047 \pm 0.004 \mu\text{m}^2 \text{s}^{-1}$  (Fig. 5D). This result is in good agreement with a recent report of cadherin diffusion in cell-cell junctions.<sup>49</sup> Taken together, the dynamic assembly of N-cadherin chimera underneath migrating cells highlights the potential of polymer-tethered multi-bilayer systems as cell surface-mimicking substrates.

The observed accumulation process of N-cadherin chimera in Fig. 5, which is profoundly different from the behavior of linkers chemically conjugated to a polymeric gel substrate, can be attributed to the lateral mobility of single N-cadherin chimera in the multi-bilayer system described in Fig. 2B. Here, we show that dye-labeled N-cadherin chimera are particularly enriched at the periphery of the cell body and at cellular extensions (Fig. 5C). Interestingly, Biswas *et al.* recently reported a similar enrichment of E-cadherin chimera at the periphery of the cell body of MKN-28 cells adsorbed to a solid-supported lipid

bilayer of high viscosity (low lipid mobility).<sup>27</sup> Their study is notable because it confirmed the importance of cytoskeletal processes in the detected E-cadherin accumulation process. The ability to accumulate linkers in a linker-functionalized polymer-tethered lipid multi-bilayer leads to a rather weak influence of linker density on cell spreading. Specifically, our work determines that changes in N-cadherin chimera linker concentration associated with average linker distances of 48 and 68 nm have no notable influence on the spreading area of C2C12 myoblasts on the biomembrane-mimicking cell substrate (Fig. 4B and C). In contrast, polymeric substrates with chemically conjugated linkers are known to exhibit enhanced cell spreading with increasing linker density below a critical linker distance of  $\sim 70$  nm.<sup>43</sup>

### Cytoskeletal forces of plated cells cause formation and mobility of bilayer-bound N-cadherin chimera clusters

Fig. 6A–E provides complementary information about the time evolution of N-cadherin chimera linker distribution underneath adherent cells. Specifically, the distribution of fluorescently tagged N-cadherin chimera in the polymer-tethered membrane system is monitored over time in selected regions at the front and tail of the cell (indicated by red frames in Fig. 6A). Here, Fig. 6B and C show the time evolution of the N-cadherin chimera distribution at the cell's front, whereas (Fig. 6D and E) provide corresponding data from the tail region. As Fig. 6B and C (front) and Fig. 6D and E (tail) demonstrate, N-cadherin chimera clusters are not static, both regions are characterized by substantial long-range movements of N-cadherin chimera patches with remarkable parallels to long-range movements of cadherin linkages between polarized cells.<sup>7,8</sup>

As confirmed in the N-cadherin chimera-functionalized fluorescent bead assay in Fig. 3, N-cadherin chimera clusters are not expected to diffuse on their own in a polymer-tethered membrane system. Therefore, the observed long-range movement

of N-cadherin chimera patches in Fig. 6A–E suggests the involvement of cell-generated forces. Indeed, addition of 20  $\mu$ M blebbistatin, a myosin II inhibitor, caused the immobilization and subsequent dissolution of N-cadherin chimera clusters (Fig. 6F–I), illustrating the significance of the cytoskeleton in N-cadherin linker cluster formation and mobility. The long-range movement of cell-substrate linkages in a linker-functionalized polymer-tethered multi-bilayer is intriguing in light of the previously reported AJ dynamics in multi-cellular systems, which include basal-to-apical cadherin flow at cellular junctions of polarized cells<sup>7</sup> and actin-dependent AJ treadmilling.<sup>8</sup> Interestingly, in a cell cluster, only protruding cells seem to form linkages between AJ and cytoskeleton, suggesting an intriguing interplay between AJ dynamics and asymmetric cytoskeleton organization during cell protrusion in a cell cluster.<sup>7</sup> Consequently, the ability to replicate linker dynamics and long-range cell-substrate linkage mobility without hindering cell migration makes the N-cadherin chimera-functionalized polymer-tethered single/multi-bilayer system a more realistic surface-mimicking substrate than linker-functionalized polymeric substrates.

### Number of stacked bilayers in N-cadherin chimera-functionalized polymer-tethered multi-bilayer influences morphology, cytoskeletal organization, adhesion formation, and traction forces of plated cells

Previously, we established that changes in bilayer stacking in a laminin-functionalized polymer-tethered multi-bilayer system alter fibroblast morphology, cytoskeletal organization, and focal adhesion formation.<sup>28,29</sup> Similarly, the representative immunofluorescence micrographs in Fig. 7 demonstrate that changes in bilayer stacking have a notable impact on both the cytoskeletal organization and AJ formation of C2C12 myoblasts adhered to a comparable cell substrate *via* N-cadherin linkages. As Fig. 7A illustrates, myoblasts on a single bilayer frequently display polygonic morphologies with well-developed ventral stress fibers,

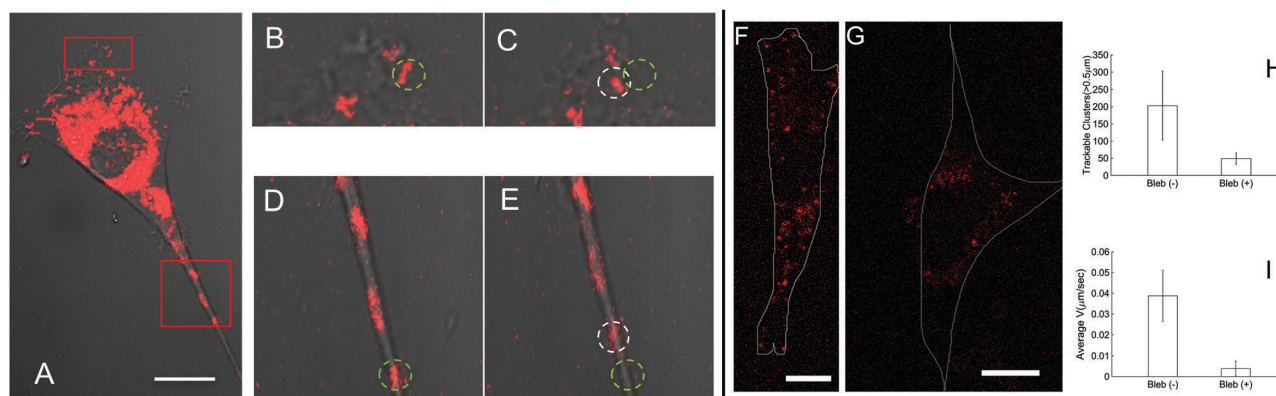


**Fig. 6** Representative spatiotemporal analysis of Alexa 555-labeled N-cadherin chimera underneath a C2C12 myoblast (A) shows long-range mobility of chimera clusters at front (B and C), and tail regions (D and E) of the cell. Enlarged areas are indicated by red rectangles (A). Green and White circles illustrate N-cadherin cluster positions at times  $t = 0$  s (green) and  $t = 40$  s (white), respectively. Visible clusters of N-cadherin chimera underneath adhered C2C12 myoblasts (F) largely disappear upon treatment with 20  $\mu$ M blebbistatin (bleb) for 30 min (G). Tracking analysis of N-cadherin clusters using the Matlab-based tracking program uTrack, which was made freely available by the Danuser lab,<sup>50</sup> demonstrates that blebbistatin treatment significantly reduces both the number of trackable clusters (set tracking size threshold: 0.5  $\mu$ m) (H) and cluster mobility (I). Error bars indicate standard deviation ( $P < 0.005$  from two-time ANOVA test). Scale bars: 20  $\mu$ m.

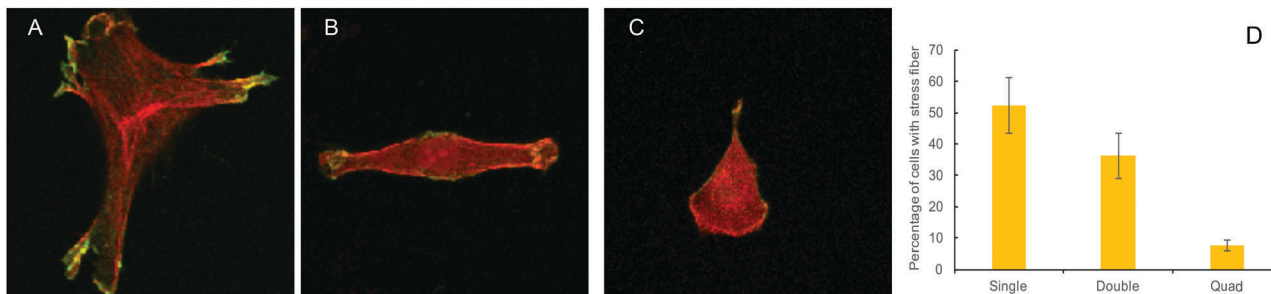


Fig. 7 Representative immunofluorescence micrographs display markedly different changes in myoblast spreading, as well as actin (red channel) and  $\beta$ -catenin (green channel) distributions on N-cadherin functionalized single (A), double (B), and quadruple bilayers (C). Increasing bilayer stacking leads to decreasing population of stress fiber-forming cells (D). Micrographs size:  $50\ \mu\text{m} \times 50\ \mu\text{m}$ . Error bars in (D) represent standard deviation of 3 sets of 30 cells for each sample.

which span the whole cell (red channel). In this case, corresponding analysis of  $\beta$ -catenin distribution (green channel) suggests formation of well-developed AJs. In contrast, on multi-bilayer substrates, myoblasts of triangular or spindle shapes become prevalent, which lack visible actin stress fibers and show less pronounced AJs (Fig. 7B and C). Analysis of actin stress fiber formation has been a useful measure to probe the extent of cell-generated forces on substrates of different stiffness.<sup>51</sup> Therefore, the extent of actin stress fiber formation of plated C2C12 cells was quantitatively analyzed as a function of bilayer stacking. Fig. 7D shows that the percentage of stress fiber-forming cells decreases with bilayer stacking on linker-functionalized multi-bilayer substrates, which is in good agreement with comparable results of fibroblasts on corresponding biomembrane-mimicking cell substrates with laminin linkers.<sup>29</sup>

In another set of experiments, we explored the influence of bilayer stacking on the cell migration speed of C2C12 myoblasts on polymer-tethered single/multi-bilayer substrates carrying N-cadherin chimera linkers (Fig. 8). As described in the Materials and methods section, cell migration data were obtained by acquiring confocal micrographs of plated cells every 5 min over a time period of 2 h and by tracking the nucleus of migrating cells over time. As Fig. 8 illustrates, C2C12 myoblasts are able

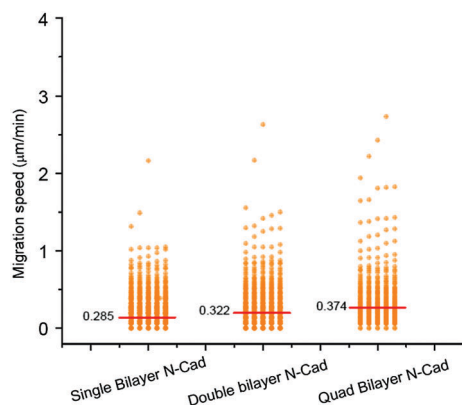


Fig. 8 C2C12 myoblasts show increasing migration speed with increasing degree of stacking on N-cadherin functionalized polymer-tethered multi-bilayer system. Red lines illustrate average values.

to migrate on a N-cadherin chimera-functionalized single/multi-bilayer system. Moreover, Fig. 8 also shows that the cell migration velocity gradually increases with stacking, which is in good agreement with comparable data of 3T3 fibroblasts on polymer-tethered single/multi-bilayers with laminin linkers.<sup>29</sup> It should be noted that corresponding fibroblast motility data on the basis of mean-square-displacement analysis over a longer time period of 6 h revealed a slightly opposite trend. However, this discrepancy has been attributed to the fact that slow cells with a more super-diffusive and persistent movement can outrun all other cells.<sup>28</sup>

Next, cellular tractions were probed on a FN-coated 6.1% PAA gel (used as reference), as well as on comparable gels with N-cadherin chimera-functionalized single and triple bilayer systems. As representative traction force maps reveal, cellular tractions are highest on the PAA gel without single/multi-bilayer coating (Fig. 9A), intermediate in cells on a single bilayer substrate (Fig. 9B), and lowest in cells on a triple bilayer (Fig. 9C). Fig. 9D shows calculated strain energies, a scalar measure of the total cell traction forces. The strain energy data in Fig. 9D demonstrate that maximum cellular tractions occur on FN-coated 6.1% PAA gels, while addition of the biomembrane-mimicking cell substrate leads to a reduction of cell tractions. Intriguingly, the single and triple bilayer data in Fig. 9D also show that increases in bilayer stacking lead to a substantial decrease in cellular traction forces, comparable to recent findings of fibroblasts plated on laminin-functionalized bilayer substrates of comparable stacking.<sup>28</sup> Overall, the traction force data in Fig. 9 are consistent with the actin stress fiber formation and motility data in Fig. 7 and 8.

Together the results in Fig. 7–9 highlight a key feature of the polymer-tethered lipid multi-bilayer system, namely the ability to alter substrate mechanical properties by altering the degree of bilayer stacking. Indeed, recent magnetic tweezer experiments on laminin-coated polymer-tethered multi-bilayers not only confirmed the overall elastic response of polymer-tethered multi-bilayers with respect to adsorbed beads mimicking cellular adhesions, but also demonstrated that systematic variation of the degree of bilayer stacking is associated with changes in substrate compliance without altering the dissipative part of the substrate response.<sup>28</sup> Consistent with these findings, here we

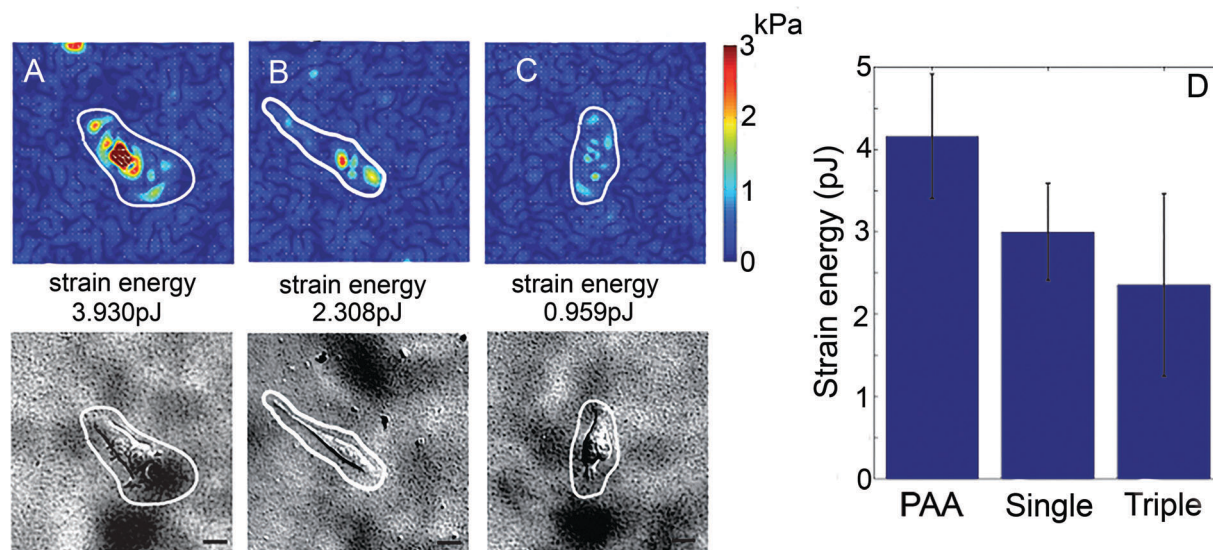


Fig. 9 Traction force maps of myoblasts on traditional FN-coated PAA gel (A) and N-cadherin functionalized single (B), and triple bilayers (C) demonstrate reduction of cellular traction forces with increasing degree of stacking, as shown by resulting strain energy values (D). Scale bar: 20  $\mu\text{m}$ . Strain energy values obtained from 20 cells for each bilayer sample; error bars represent standard deviation.

demonstrate that key properties of cellular mechanosensitivity of plated C2C12 myoblasts can be altered by changing substrate stiffness (degree of bilayer stacking) in a N-cadherin-functionalized polymer-tethered lipid multi-bilayer. For example, the immunofluorescence data of actin and  $\beta$ -catenin distribution in Fig. 7A–C illustrate that increases in bilayer stacking lead to reduced actin stress fiber formation and less pronounced AJs. Changes in bilayer stacking also influence cell migration speed (Fig. 8). The ability to alter substrate stiffness *via* the degree of bilayer stacking is furthermore demonstrated by traction force microscopy experiments on N-cadherin-functionalized polymer-tethered multi-bilayer systems. These experiments identify reduced cellular traction forces with increasing number of bilayers in the stack (Fig. 9), which are consistent with the obtained actin stress fiber and AJs size data. The above findings, which are in good agreement with previous results of 3T3 fibroblasts on laminin-coated polymer-tethered multi-bilayers,<sup>28,29</sup> highlight the great potential of linker-functionalized polymer-tethered multi-bilayers as cell surface-mimicking substrate for the analysis of cellular mechanosensitivity.

It should be emphasized that the demonstrated potential of the linker-functionalized polymer-tethered multi-bilayer as cell surface-mimicking substrate for the analysis of cellular mechanosensitivity critically depends on the presence of polymer-tethered lipids (lipopolymers) in such a membrane system. For example, analysis of the lateral diffusion of lipids and membrane proteins in a polymer-tethered phospholipid bilayer previously showed that lipopolymers act as diffusion obstacles, thereby causing the obstruction of lateral diffusion of membrane constituents in a size-dependent manner.<sup>40</sup> Consistent with these findings, here we report that individual N-cadherin chimera linkers and linker clusters exhibit qualitatively different behavior in the polymer-tethered lipid multi-bilayer system. While, single N-cadherin chimera linkers are laterally mobile in such a biomembrane

mimetic (Fig. 2), corresponding linker clusters are unable to diffuse on their own in the same membrane system (Fig. 3). This peculiar behavior explains why individual N-cadherin chimera linkers are able to assemble into linker clusters underneath plated cells, enabling the formation of stable N-cadherin linkages between adherent cells and substrate. It also clarifies why adherent cells show cellular tractions, spreading, and migration on N-cadherin chimera-functionalized polymer-tethered lipid multi-bilayers, whereas cell spreading/migration is suppressed on a supported fluid lipid bilayer without lipopolymers.<sup>25</sup> The remarkable tunability of substrate stiffness *via* the degree of bilayer stacking can be attributed to the intricate inter-bilayer coupling mechanisms in polymer-tethered lipid multi-bilayers. These coupling mechanisms include the previously reported slaved lipid diffusion, strong inter-leaflet coupling of obstructed diffusion, and formation of lipopolymer-enriched inter-bilayer connections.<sup>41,52,53</sup>

## Conclusion

In the current work, we demonstrate that C2C12 myoblasts are able to spread and migrate on N-cadherin chimera-functionalized polymer-tethered lipid multi-bilayers without impairing the integrity of these biomembrane-mimicking cell substrates. Unlike traditional polymeric gel substrates with polymer-conjugated linkers, polymer-tethered lipid multi-bilayers enable the dynamic assembly of N-cadherin chimera linkers into linker clusters and the long-range movement of cadherin-based cell-substrate linkages underneath migrating cells. Such behavior shows remarkable parallels to the linker dynamics observed between cells in a cell cluster.<sup>7</sup> These fascinating linker properties during cell migration can be attributed to the presence of lipopolymers in the polymer-tethered single/multi-bilayer system, which hinder

the lateral mobility of linker clusters, but not of single linkers. Consequently, cells on N-cadherin chimera-functionalized polymer-tethered single/multi-bilayers are able to transmit traction forces *via* dynamically assembled linker clusters to the underlying substrate, a requirement for cell spreading/migration to occur. In addition, the adjustability of substrate stiffness by the degree of multi-bilayer stacking, a hallmark of polymer-tethered lipid multi-bilayers, provides an attractive tool to examine cellular mechanosensitivity. Because the presented experimental cell-substrate platform replicates important processes at cell-cell junctions in a more physiological way than other available engineered cell substrates, we anticipate its use for studying cellular mechanosensitivity and mechanobiology in a multi-cellular environment.

## Acknowledgements

This work was in part supported by the National Science Foundation (grant: DMR 1006552), the IUPUI Integrated Nano-systems Development Institute, and the German Science Foundation (DFG).

## References

- D. A. Lauffenburger and A. F. Horwitz, *Cell*, 1996, **84**, 359–369.
- C. G. Galbraith, K. M. Yamada and M. P. Sheetz, *J. Cell Biol.*, 2002, **159**, 695–705.
- B. Ladoux, E. Anon, M. Lambert, A. Rabodzey, P. Hersen, A. Buguin, P. Silberzan and R. M. Mege, *Biophys. J.*, 2010, **98**, 534–542.
- Z. Liu, J. L. Tan, D. M. Cohen, M. T. Yang, N. J. Sniadecki, S. A. Ruiz, C. M. Nelson and C. S. Chen, *Proc. Natl. Acad. Sci. U. S. A.*, 2010, **107**, 9944–9949.
- C. M. Regen and A. F. Horwitz, *J. Cell Biol.*, 1992, **119**, 1347–1359.
- C. Ballestrem, B. Hinz, B. A. Imhof and B. Wehrle-Haller, *J. Cell Biol.*, 2001, **155**, 1319–1332.
- Y. Kametani and M. Takeichi, *Nat. Cell Biol.*, 2007, **9**, 92–98.
- F. Peglion, F. Llense and S. Etienne-Manneville, *Nat. Cell Biol.*, 2014, **16**, 639–651.
- N. Q. Balaban, U. S. Schwarz, D. Riveline, P. Goichberg, G. Tzur, I. Sabanay, D. Mahalu, S. Safran, A. Bershadsky, L. Addadi and B. Geiger, *Nat. Cell Biol.*, 2001, **3**, 466–472.
- C. S. Chen, J. Tan and J. Tien, *Annu. Rev. Biomed. Eng.*, 2004, **6**, 275–302.
- R. Zaidel-Bar, S. Itzkovitz, A. Ma'ayan, R. Iyengar and B. Geiger, *Nat. Cell Biol.*, 2007, **9**, 858–868.
- H. Wolfenson, I. Lavelin and B. Geiger, *Dev. Cell*, 2013, **24**, 447–458.
- O. Thoumine, M. Lambert, R. M. Mege and D. Choquet, *Mol. Biol. Cell*, 2006, **17**, 862–875.
- J. L. Alonso and W. H. Goldmann, *AIMS Biophys.*, 2016, **3**, 50–62.
- D. E. Discher, P. Janmey and Y. L. Wang, *Science*, 2005, **310**, 1139–1143.
- V. Vogel and M. Sheetz, *Nat. Rev. Mol. Cell Biol.*, 2006, **7**, 265–275.
- D. E. Ingber, *Ann. Med.*, 2003, **35**, 564–577.
- D. E. Jaalouk and J. Lammerding, *Nat. Rev. Mol. Cell Biol.*, 2009, **10**, 63–73.
- A. J. Engler, S. Sen, H. L. Sweeney and D. E. Discher, *Cell*, 2006, **126**, 677–689.
- B. Ladoux, W. J. Nelson, J. Yan and R. M. Mege, *Integr. Biol.*, 2015, **7**, 1109–1119.
- R. J. Pelham, Jr. and Y. Wang, *Proc. Natl. Acad. Sci. U. S. A.*, 1997, **94**, 13661–13665.
- A. Chopra, E. Tabdanov, H. Patel, P. A. Janmey and J. Y. Kresh, *Am. J. Physiol.: Heart Circ. Physiol.*, 2011, **300**, H1252–H1266.
- J. C. M. Vega, M. K. Lee, J. H. Jeong, C. E. Smith, K. Y. Lee, H. J. Chung, D. E. Leckband and H. Kong, *Biomacromolecules*, 2014, **15**, 272–279.
- J. T. Groves, L. K. Mahal and C. R. Bertozzi, *Langmuir*, 2001, **17**, 5129–5133.
- T. D. Perez, W. J. Nelson, S. G. Boxer and L. Kam, *Langmuir*, 2005, **21**, 11963–11968.
- A. P. Kourouklis, R. V. Lerum and H. Bermudez, *Biomaterials*, 2014, **35**, 4827–4834.
- K. H. Biswas, K. L. Hartman, C. H. Yu, O. J. Harrison, H. Song, A. W. Smith, W. Y. Huang, W. C. Lin, Z. Guo, A. Padmanabhan, S. M. Troyanovsky, M. L. Dustin, L. Shapiro, B. Honig, R. Zaidel-Bar and J. T. Groves, *Proc. Natl. Acad. Sci. U. S. A.*, 2015, **112**, 10932–10937.
- L. A. Lautscham, C. Y. Lin, V. Auernheimer, C. A. Naumann, W. H. Goldmann and B. Fabry, *Biomaterials*, 2014, **35**, 3198–3207.
- D. E. Minner, P. Rauch, J. Kas and C. A. Naumann, *Soft Matter*, 2014, **10**, 1189–1198.
- D. E. Minner, V. L. Herring, A. P. Siegel, A. Kimble-Hill, M. A. Johnson and C. A. Naumann, *Soft Matter*, 2013, **9**, 9643–9650.
- C. T. Mierke, P. Kollmannsberger, D. P. Zitterbart, G. Diez, T. M. Koch, S. Marg, W. H. Ziegler, W. H. Goldmann and B. Fabry, *J. Biol. Chem.*, 2010, **285**, 13121–13130.
- T. M. Koch, S. Munster, N. Bonakdar, J. P. Butler and B. Fabry, *PLoS One*, 2012, **7**, e33476.
- A. P. Siegel, A. Kimble-Hill, S. Garg, R. Jordan and C. A. Naumann, *Biophys. J.*, 2011, **101**, 1642–1650.
- N. F. Hussain, A. P. Siegel, Y. Ge, R. Jordan and C. A. Naumann, *Biophys. J.*, 2013, **104**, 2212–2221.
- M. Kang, M. Andreani and A. K. Kenworthy, *PLoS One*, 2015, **10**, e0127966.
- C. Raupach, D. P. Zitterbart, C. T. Mierke, C. Metzner, F. A. Muller and B. Fabry, *Phys. Rev. E: Stat., Nonlinear, Soft Matter Phys.*, 2007, **76**, 011918.
- J. P. Butler, I. M. Tolic-Norrelykke, B. Fabry and J. J. Fredberg, *Am. J. Physiol.: Cell Physiol.*, 2002, **282**, C595–C605.
- S. F. Fenz, R. Merkel and K. Sengupta, *Langmuir*, 2009, **25**, 1074–1085.
- C. Hogan, N. Serpente, P. Cogram, C. R. Hosking, C. U. Bialucha, S. M. Feller, V. M. Braga, W. Birchmeier and Y. Fujita, *Mol. Cell Biol.*, 2004, **24**, 6690–6700.

- 40 M. A. Deverall, E. Gindl, E. K. Sinner, H. Besir, J. Ruehe, M. J. Saxton and C. A. Naumann, *Biophys. J.*, 2005, **88**, 1875–1886.
- 41 M. A. Deverall, S. Garg, K. Ludtke, R. Jordan, J. Ruhe and C. A. Naumann, *Soft Matter*, 2008, **4**, 1899–1908.
- 42 P. Mascalchi, E. Haanappel, K. Carayon, S. Mazerès and L. Salomé, *Soft Matter*, 2012, **8**, 4462–4470.
- 43 M. Arnold, E. A. Cavalcanti-Adam, R. Glass, J. Blummel, W. Eck, M. Kantelehner, H. Kessler and J. P. Spatz, *ChemPhysChem*, 2004, **5**, 383–388.
- 44 H. Colognato, D. A. Winkelmann and P. D. Yurchenco, *J. Cell Biol.*, 1999, **145**, 619–631.
- 45 S. Garg, S. C. Fischer, E. M. Schuman and E. H. Stelzer, *J. R. Soc., Interface*, 2015, **12**, 20141055.
- 46 R. M. Mege, J. Gavard and M. Lambert, *Curr. Opin. Cell Biol.*, 2006, **18**, 541–548.
- 47 S. Hong, R. B. Troyanovsky and S. M. Troyanovsky, *J. Cell Biol.*, 2011, **192**, 1073–1083.
- 48 D. Schmidt, T. Bihl, S. Fenz, R. Merkel, U. Seifert, K. Sengupta and A. S. Smith, *Biochim. Biophys. Acta*, 2015, **1853**, 2984–2991.
- 49 M. Causeret, N. Taulet, F. Comunale, C. Favard and C. Gauthier-Rouviere, *Mol. Biol. Cell*, 2005, **16**, 2168–2180.
- 50 K. Jaqaman, D. Loerke, M. Mettlen, H. Kuwata, S. Grinstein, S. L. Schmid and G. Danuser, *Nat. Methods*, 2008, **5**, 695–702.
- 51 T. Yeung, P. C. Georges, L. A. Flanagan, B. Marg, M. Ortiz, M. Funaki, N. Zahir, W. Ming, V. Weaver and P. A. Janmey, *Cell Motil. Cytoskeleton*, 2005, **60**, 24–34.
- 52 H. E. Warriner, S. H. Idziak, N. L. Slack, P. Davidson and C. R. Safinya, *Science*, 1996, **271**, 969–973.
- 53 L. Zhang and S. Granick, *Proc. Natl. Acad. Sci. U. S. A.*, 2005, **102**, 9118–9121.